

Allocation for Omnidirectional Aerial Robots: Incorporating Power Dynamics

Eugenio Cuniato, *Student Member, IEEE*, Mike Allenspach, *Student Member, IEEE*, Thomas Stastny, *Member, IEEE*, Helen Oleynikova, *Member, IEEE*, Roland Siegwart, *Fellow, IEEE*, Michael Pantic, *Member, IEEE*,

Abstract—Tilt-rotor aerial robots are more dynamic and versatile than their fixed-rotor counterparts, since the thrust vector and body orientation are decoupled. However, the coordination of servomotors and propellers (the *allocation* problem) is not trivial, especially accounting for overactuation and actuator dynamics. We present and compare different methods of actuator allocation for tilt-rotor platforms, evaluating them on a real aerial robot performing dynamic trajectories. We extend the state-of-the-art geometric allocation into a differential allocation, which uses the platform’s redundancy and does not suffer from singularities typical of the geometric solution. We expand it by incorporating actuator dynamics and introducing propeller *limit curves*. These improve the modeling of propeller limits, automatically balancing their usage and allowing the platform to selectively activate and deactivate propellers during flight. We show that actuator dynamics and limits make the tuning of the allocation not only easier, but also allow it to track more dynamic oscillating trajectories with angular velocities up to 4 rad s^{-1} , compared to 2.8 rad s^{-1} of geometric methods.

Index Terms—Aerial Systems: Mechanics and Control, Direct/Inverse Dynamics Formulation, Motion Control, Omnidirectional Aerial Robots

I. INTRODUCTION

Omnidirectional Aerial Robots have enjoyed increasing interest in the aerial robotics community [1]. The actuation capabilities of these systems allow omnidirectional thrust generation, resulting in fully-decoupled translational and rotational dynamics. Recent works on aerial physical interaction demonstrate the superiority of omnidirectional platforms over traditional underactuated ones, ensuring precise motion and interaction force control with simultaneous disturbance rejection [2]. Depending on the specifics of the actuation, omnidirectional aerial robots can be classified as either *fixed-rotor* or *tilt-rotor* platforms. Fixed-rotor describes aerial robot system morphologies with propellers mounted rigidly at specific angles [3]–[6]. Although mechanically simple, their flight efficiency is limited due to the significant amount of internal forces. As such, selecting appropriate rotor mounting angles is not trivial and poses a trade-off between prolonging flight duration and promoting lateral force generation capabilities for interaction.

All authors are with the Autonomous Systems Lab (ASL), ETH Zurich. Corresponding author: ecuniato@ethz.ch.

The research leading to these results has been supported by the AERO-TRAIN project, European Union’s Horizon 2020 research and innovation program under the Marie Skłodowska-Curie grant agreement No 953454 and the ETH RobotX Research Program. The authors are solely responsible for its content.



Fig. 1: The Omnidirectional Aerial Robot hovering at a tilted configuration. All the experiments are executed on this platform.

Instead, tilt-rotor vehicles make use of dedicated actuators to modify the propeller orientation, depending on the task at hand [7]–[10]. This versatility strongly promotes their use in aerial interaction applications, where transitioning between an efficient navigation and a high-force interaction configuration might be required at different points throughout the mission [2], [11]. However, it requires elaborate control allocation schemes to handle potential singularities, resolve actuator redundancy and respect the difference in dynamic response between tilt-motor and the propellers.

Aiming to address these challenges and further enhance the capabilities of tilt-rotor robots, we propose, compare and discuss different control allocation methodologies for the tilt-rotor platform shown in Fig. 1. Particular focus lies on how to include the different actuator dynamics and limits into the problem, exploit the system’s high overactuation with secondary task objectives (like balancing propeller speeds or commanding specific arm motions), and smoothly turning off propellers during flight, opening the door to new crash-resilience and aerial manipulation scenarios.

A. Related Works

Considering their primary use-case as aerial manipulators, modern tilt-rotor aerial robots are mechanically designed to optimize omnidirectional force/torque envelopes, while exhibiting a dominant hover orientation for efficient flight. As shown in [8], this optima is achieved by following a standard multi-copter morphology, meaning all propellers are mounted in a co-planar and symmetric fashion on the main body. Unlike standard under-actuated multi-copters however, the direction of each propeller axes can be adjusted in flight, due to actuated tilting joints at these mounting points. Given a desired total force/torque to be acting on the vehicle (e.g. for trajectory tracking or force control), solving the allocation problem thus boils down to determining the required propeller speed and direction for each rotor. In the following we summarize common solutions in the literature of tri- [7], quad- [10], [12]–[14] and hexa-copter-like [2], [8], [9], [15]–[19] platforms.

Motivated by the comparatively slow tilt dynamics, [15] proposes to optimize tilt angles along a given trajectory for efficient flight before the start of each mission, but then keeping them constant during execution. To still ensure accurate tracking in the presence of disturbances, only the propeller speeds are updated online using a well-known matrix-inversion-based allocation scheme [20]. Aside from requiring knowledge of the full task trajectory ahead of time, naively optimizing tilt angles for efficiency can result in singularities and loss of omnidirectionality [18]. Follow-up works [9], [16], [17] address this limitation by proposing to employ an online tilt angle planner instead. While also separately allocating tilt angles and rotor speeds, such a planner would aim to prevent singularities, without introducing excessive internal forces that reduce efficiency. However, the choice of tilt angle in different flight situations seem to be very much task dependent and heuristically defined by the user. In short, incorporating control authority and efficient flight while avoiding singularities is not trivial when tilt angle and propeller speed allocation are performed separately.

Alternatively, control allocation of both tilt angles and rotor speeds can be combined, resulting in a nonlinear and potentially high-dimensional system of equations to be solved. Approaches presented in [7], [12], [19], [21]–[23] demonstrate how propeller force decomposition and trigonometric identities can produce a linear formulation suitable for matrix-inversion-based *geometric allocation* schemes (see Sec III). Since the matrix becomes ill-conditioned when the system approaches a singular configuration, singularity cases must be analyzed and handled carefully. Possible heuristics are proposed and experimentally validated in [19], for example adding a bias to the desired arm angles to avoid ending up in singular configurations. However, the mathematical problem of mapping a desired wrench to tilt angles and rotor speeds still intrinsically suffers from singularities.

It should be noted that the cited works often neglect the different dynamics between propellers and servomotors [2], which can result in degraded disturbance rejection and dynamic tracking (see Sec. VIII).

To better coordinate the tilting motion and propeller dynam-

ics, recent works propose to control the tilt angle *velocities* and rotor *accelerations* to recreate a desired change in total body force and torque, rather than forces and torques themselves. In other words, to move the allocation problem to a higher differential level [8], [13]. This so-called *differential allocation* (see Sec IV) is not only more realistic in terms of actuator dynamics (as we no longer assume an instantaneous change of tilt angles and rotor speeds), but is also inherently robust to singularities [8]. Furthermore, resolution of the actuator redundancy through nullspace exploitation is straightforward, for example to improve efficiency [13] or for consideration of mechanical constraints [8]. While promising, existing differential allocation methods require measuring translational and rotational body accelerations, which are hard to obtain at sufficient quality from standard on-board sensor suites. If linear accelerations are available, from accelerometer data, they are usually subject to a non-negligible amount of noise and are hard to filter at the required controller frequencies. Model-based estimation also proves difficult, since airflow interaction and aerodynamic interference between rotor blades complicate the system modeling. Moreover, these methods always require the use of posture nullspace objectives even just for free-flight, which keeps the nullspace always full and requires task switching in case a change in the nullspace goals is needed [24] (e.g. from efficiency to mechanical constraints or manipulation tasks).

Despite the potential of differential control allocation for aerial robots, there are still multiple gaps in the existing literature. Firstly, performance is highly dependent on the availability and quality of 6degrees of freedom (DOF) body acceleration measurements or estimates. Secondly, actuator dynamics (and especially their limits) are never explicitly considered in the allocation problem, or at best as simple integrators. Moreover, balancing the propeller speeds and thus energy efficiency always requires the use of nullspace objectives, which complicates the control architecture and requires task switching. Finally, despite high-level discussions about its apparent advantages, in-depth comparison between differential and geometric control allocation schemes are missing.

B. Contributions

In this work, we compare multiple allocation methods and propose a method to embed the different actuator properties and desired behaviors into one differential allocation theory.

- We improve the state-of-the-art differential allocation: we remove the requirement of acceleration feedback, improving its trajectory-tracking performance and enabling its use in common wrench-based robot control architectures.
- We make the differential allocation aware of its actuator limits and dynamics, improving the mathematical conditioning of the problem and showing increased stability during aggressive flight trajectories.
- We introduce and embed propellers' limit curves into the allocation description, providing a powerful new tool for optimizing flight efficiency and desired propeller speeds, without the use of secondary allocation goals.
- We also show how these curves can be used to turn off propellers in flight, allowing the platform to control its

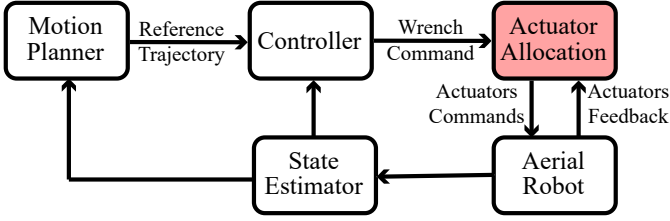


Fig. 2: A general control architecture for aerial robots. The pose controller compares the current odometry to a reference trajectory and produces a wrench command. The wrench command is finally allocated to the actuators of the robot, namely servomotors and propellers, to generate the desired wrench which drives the platform. In this work we focus on the allocation block, highlighted in red.

propelling arms as manipulation tools, possibly removing the need for additional manipulation arms.

We thus propose a new actuator allocation method that outperforms past geometric and differential allocations in terms of stability and dynamic tracking performance, doesn't require acceleration feedback, and allows us to use the propelling arms for any arbitrary secondary task, not necessarily flight related.

II. SYSTEM ARCHITECTURE

Our tilt-rotor aerial robot has six arms which can independently rotate around their axis using six servomotors. Each arm mounts one rotor at its tip, creating an independent thrust unit. With a total of six arms and propellers, the robot has twelve DOFs, and it is able to separate position and orientation control in space. A common control architecture is illustrated in Fig. 2. Given a set of sensors available on aerial robots (GPS, IMU, Lidar, optical flow, ...), the state estimator provides an odometry measure [25], which the controller [2] uses to generate a command/wrench (forces and torques) to follow the current position and/or velocity reference. Finally, the command wrench $w \in \mathbb{R}^6$ is transformed into actuator commands for the platform's arm angles $\alpha = [\alpha_0, \dots, \alpha_{N-1}]^T$ and propeller speeds $\omega = [\omega_0, \dots, \omega_{N-1}]^T$ through the chosen allocation method, with $N \in \mathbb{R}$ the number of arms.

In the following sections, we will keep the motion planner, controller and state estimator fixed as in [2], and focus on the actuator allocation problem. We will compare the state-of-the-art geometric allocation method with the proposed differential allocation, and show how the latter can be improved by integrating the actuator dynamics and limits into the problem. A schematic of the allocation methods that will be introduced in the following sections can be seen in Fig. 3.

III. GEOMETRIC ALLOCATION (GE)

For the reader's convenience, here we reproduce the state-of-the-art geometric allocation method of [26], which only uses the platform's geometry to map the desired control

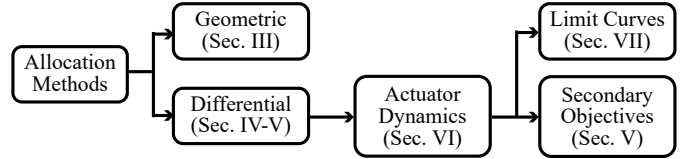


Fig. 3: The evolution of allocation methods, from the basic geometric allocation, to the differential and its extensions.

wrench into propeller speeds and arm rotation angles. [26] defines the allocation problem as

$$w = Au, \quad u = \begin{bmatrix} \omega_0 \sin \alpha_0 \\ \omega_0 \cos \alpha_0 \\ \dots \\ \omega_{N-1} \sin \alpha_{N-1} \\ \omega_{N-1} \cos \alpha_{N-1} \end{bmatrix}, \quad (1)$$

where $A \in \mathbb{R}^{6 \times 2N}$ represents a constant allocation matrix depending only on the system's geometry, while $u \in \mathbb{R}^{2N}$ is the result of the allocation, obtained pseudoinverting the matrix A . Once the command vector u is generated, we extract the actual rotor speeds and tilt angles with

$$\alpha_i = \text{atan2}(u_{2i}, u_{2i+1}), \quad \forall i = 0 \dots N-1 \quad (2a)$$

$$\omega_i = \sqrt{u_{2i}^2 + u_{2i+1}^2}, \quad \forall i = 0 \dots N-1. \quad (2b)$$

This method, which takes inspiration from the allocation of standard aerial robots, has the advantage of only requiring knowledge of the system's geometry. However, it has a few limitations:

- Since the allocation is purely geometric, it does not account for actuator dynamics or limits.
- The matrix A is constant and full rank, but the allocation problem can become singular depending on the desired wrench [26], i.e., it's not always possible to extract angles α and rotor speeds ω with Eq. (2).
- The geometric allocation does not exploit the system's redundancy, only providing the solution with the minimum rotor speeds.

To overcome some of these limitations, [8] introduced a differential allocation method.

IV. DIFFERENTIAL ALLOCATION

The idea is to differentiate the relation in Eq. (1) to map the time derivative of the wrench command (which we will from now on refer to as *jerk*) to arm tilting speed and propeller acceleration, as

$$\dot{w} = AD(q)\dot{q} = J(q)\dot{q}, \quad (3)$$

where $\dot{w} \in \mathbb{R}^6$ is the desired jerk to apply on the robot's body, $q = [\alpha^T, \omega^T]^T \in \mathbb{R}^{2N}$ is the vector of joint states and $D = \frac{\partial u}{\partial q} \in \mathbb{R}^{2N \times 2N}$ is the Jacobian of the geometric actuation vector u . The solution to this allocation problem is then

$$\dot{q} = J^\ddagger \dot{w} + (I_{2N} - J^\ddagger J)\dot{q}^*, \quad (4)$$

where the allocation's output is now a vector $\dot{q} \in \mathbb{R}^{2N}$ of arm rotation speeds and rotor accelerations, $\dot{q}^* \in \mathbb{R}^{2N}$ is a vector

of desired joint velocities to exploit the system's overactuation by fulfilling secondary goals, and

$$\mathbf{J}^\ddagger = \mathbf{W}^{-1} \mathbf{J}^\top (\mathbf{J} \mathbf{W}^{-1} \mathbf{J}^\top)^{-1}, \quad (5)$$

a weighted pseudoinverse of \mathbf{J} , with a positive-definite weight matrix $\mathbf{W} \in \mathbb{R}^{2N \times 2N}$ to balance between the use of tilting arms and propellers. This allocation method solves the singularity problem of the geometric solution in Section III, while enabling use of the system's overactuation with $\dot{\mathbf{q}}^*$. A possible choice for $\dot{\mathbf{q}}^*$ is to drive the propellers' speeds to a desired value (for example the hovering speed ω^*) with

$$\dot{\mathbf{q}}^* = -k_\omega [\mathbf{0}_6, (\omega_0 - \omega^*), \dots, (\omega_{N-1} - \omega^*)]^\top, \quad (6)$$

where $k_\omega \in \mathbb{R}$ is a positive gain. Other choices, like actuator limits avoidance, can be found in the literature of robot manipulators [27].

However, this allocation method has two main requirements that could limit its applicability: it allocates a jerk command and requires a weighted pseudoinverse \mathbf{W} to balance the usage between tilt angles and propellers and keep the problem numerically stable.

A. Jerk vs. Wrench Control

While the differential allocation requires a jerk command, wrench control is still the most common solution for aerial robots. Indeed, it is the natural solution to the second-order rigid body dynamics, and it only requires position and velocity feedback, both commonly available on aerial robots. The authors in [8] adopted a Linear Quadratic Regulator (LQR) to produce the control jerk from acceleration feedback. They designed two filters to obtain linear and angular acceleration feedback by filtering and differentiating Inertial Measurement Unit (IMU) data.

While this solution permits the use of a differential allocation method, its trajectory tracking performance was shown comparable with a PD controller with geometric allocation [8]. We believe the use of an LQR, too dependent on the system's model, and the quality of the acceleration feedback to be the cause of this inefficiency.

For this reason, in the following Section V we propose an augmented differential allocation, which does not require acceleration feedback and can be easily implemented with any standard wrench-based controller.

B. Weighted Pseudoinverse

To keep the problem numerically stable, the differential allocation relies on a weighted pseudoinverse, which requires manual tuning of the weight matrix \mathbf{W} to balance the usage between tilt angles and propellers. The matrix \mathbf{W} has a prominent effect on the aerial robot's behavior: too much weight on the tilt angles will push the allocation to use only the propellers, behaving the same way as a fixed multirotor, whereas too much weight on the propellers can lead the tilt angles' servomotors to rotate very fast and quickly saturate. In Section VI, we demonstrate how integrating the actuator dynamics and limits into the allocation problem can improve

its numerical conditioning without the need of a hand-tuned weight matrix.

An overview of the allocation scheme developed in the following sections is in Fig. 4.

V. AUGMENTED DIFFERENTIAL ALLOCATION (ADI)

Here we propose Augmented Differential Allocation, to bring all the advantages of the Differential Allocation in Eq. (4) to any standard wrench-based controller, without the need for acceleration feedback. We augment the input dynamics of our system in order to generate a jerk control command from a wrench command as

$$\dot{\mathbf{w}}(t) = k_j (\mathbf{w}(t) - \mathbf{w}(t-1)), \quad (7)$$

where $k_j \in \mathbb{R}$ is a gain generating a jerk proportional to the error between the current and the previous wrench commands. This approach was already validated in the context of Control Barrier Functions (CBF) for mobile robots [28] and aerial vehicles [29]. Moreover, in Section VIII we show improved trajectory tracking performance w.r.t. the geometric control architecture of [30], not only close to geometric singularities, but especially during fast and dynamic trajectories. However, it still requires tuning of the weight matrix \mathbf{W} in Eq. (5) to balance the usage between tilt angles and propellers, which ultimately still relies on user heuristics obtained in flight tests.

VI. AUGMENTED DIFFERENTIAL ALLOCATION WITH ACTUATOR LIMITS AND DYNAMICS (DLD)

To avoid these heuristics in tuning the weight matrix \mathbf{W} , we propose to balance the actuators' usage by normalizing the allocation problem with the knowledge of the actuators' control limits, instead of using a weighted pseudoinverse. We also use the actuator dynamics inside the allocation problem, by inverting them and obtaining dynamically consistent commands from the desired arm velocities and propeller accelerations. This step, usually neglected, has a significant impact on the system's dynamic performance, as presented later in the experimental results.

A. Actuator Control Limits

Consider the vectors $\underline{\dot{\mathbf{q}}} = [\underline{\dot{\boldsymbol{\alpha}}}^\top, \underline{\dot{\boldsymbol{\omega}}}^\top]^\top$ and $\bar{\mathbf{q}} = [\bar{\boldsymbol{\alpha}}^\top, \bar{\boldsymbol{\omega}}^\top]^\top$, which contain the minimum and maximum values of arm tilt angle velocity and propeller acceleration, respectively. To simplify the notation, we generally refer with *actuator velocity* $\dot{\mathbf{q}}$ to angular velocities for the tilt angles and rotor accelerations for the propellers. This is because the state of our actuators \mathbf{q} is composed of both tilt angles and rotor speeds, which can be regarded as an *actuator position*. We now normalize the actuator velocities with respect to these limits, mapping $\dot{q}_i \in [\underline{\dot{q}}_i, \bar{\dot{q}}_i]$ to $\dot{q}_{n,i} \in [-1, 1]$ with

$$\dot{q}_{n,i} = \frac{2}{\bar{\dot{q}}_i - \underline{\dot{q}}_i} \dot{q}_i - \frac{\bar{\dot{q}}_i + \underline{\dot{q}}_i}{\bar{\dot{q}}_i - \underline{\dot{q}}_i}, \quad \forall i = 0, \dots, 2N-1. \quad (8)$$

Grouping all the normalized actuator speeds together, we obtain

$$\dot{\mathbf{q}}_n = \mathbf{N} \dot{\mathbf{q}} - \mathbf{b}, \quad (9)$$

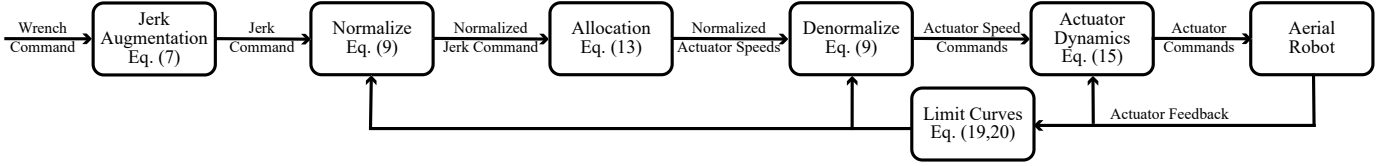


Fig. 4: The proposed differential allocation scheme. We first augment the wrench command to generate a jerk command, we then normalize it and allocate into numerically stable normalized joint speeds. Finally, we invert the actuator dynamics to obtain the desired tilt angles and propeller speeds to command the Aerial Robot.

with a diagonal scaling matrix $\mathbf{N} \in \mathbb{R}^{2N \times 2N}$ and a bias vector $\mathbf{b} \in \mathbb{R}^{2N}$, where

$$N_{i,i} = \frac{2}{\bar{q}_i - \underline{q}_i}, \quad b_i = \frac{\bar{q}_i + \underline{q}_i}{\bar{q}_i - \underline{q}_i}, \quad \forall i = 0, \dots, 2N - 1. \quad (10)$$

We now rewrite the allocation problem in Eq. (3) as a function of the normalized joint speeds $\dot{\mathbf{q}}_n$ instead of the speeds themselves $\dot{\mathbf{q}}$. Substituting Eq. (9) in Eq. (3) we obtain the normalized allocation problem

$$\dot{\mathbf{w}} = \mathbf{J}(\mathbf{q})\mathbf{N}^{-1}\dot{\mathbf{q}}_n + \mathbf{J}(\mathbf{q})\mathbf{N}^{-1}\mathbf{b}, \quad (11)$$

which is equivalent to

$$\dot{\mathbf{w}}_n = \mathbf{J}_n\dot{\mathbf{q}}_n, \quad (12)$$

where the normalized jerk command to allocate is now $\dot{\mathbf{w}}_n = \dot{\mathbf{w}} - \mathbf{J}\mathbf{N}^{-1}\mathbf{b} \in \mathbb{R}^6$ and the normalized allocation matrix is $\mathbf{J}_n = \mathbf{J}\mathbf{N}^{-1} \in \mathbb{R}^{2N \times 2N}$. Like in Eq. (4), the solution to this allocation problem is

$$\dot{\mathbf{q}}_n = \mathbf{J}_n^\dagger \dot{\mathbf{w}}_n + (\mathbf{I}_{2N} - \mathbf{J}_n^\dagger \mathbf{J}_n) \dot{\mathbf{q}}_n^*, \quad (13a)$$

$$\mathbf{J}_n^\dagger = \mathbf{J}_n^\top (\mathbf{J}_n \mathbf{J}_n^\top)^{-1}. \quad (13b)$$

Despite the similarity, this formulation has the advantage of not requiring manual tuning of a weighted pseudoinverse, but it rather induces the actuators' balancing by their velocity limits, used in Eq. (10). These can be identified on a test bench by, for example, sending a chirp setpoint signal over time, without the necessity of in-flight tuning. It also numerically conditions the allocation problem in a better way, since now the output are all quantities normalized between $[-1, 1]$ rather than tilt angle speeds $\dot{\alpha} \sim 1 \text{ rad/s}$ and propeller accelerations $\dot{\omega} \sim 10^4 \text{ rad/s}^2$ with four orders of magnitude difference.

B. Actuator Saturation

Despite normalizing the actuator commands between $[-1, 1]$, given a normalized jerk $\dot{\mathbf{w}}_n$, the allocation might still output normalized joint velocity commands $\dot{\mathbf{q}}_n$ outside of these boundaries. This can happen if the required jerk command is too high, for example when requiring very rapid maneuvers. We saturate the joint velocities between $[-1, 1]$, by linearly scaling down the velocity vector with a quantity $k_s < 1$ as

$$\text{sat}(\dot{\mathbf{q}}_n) = k_s \dot{\mathbf{q}}_n. \quad (14)$$

The desired gain is $k_s = \frac{1}{|\dot{q}_{n,b}|}$, where $\dot{q}_{n,b}$ is the biggest element of the joint speeds vector. Notice that since all the actuator commands in $\dot{\mathbf{q}}_n$ are scaled by the same quantity k_s and the relation in Eq. (12) is linear, this corresponds to

generating a jerk $\text{sat}(\dot{\mathbf{w}}_n)$ which has the same direction of the original $\dot{\mathbf{w}}_n$ but scaled in magnitude.

C. Actuator Dynamics

The normalized allocation in Eq. (13) only requires knowledge of the actuators' velocity limits but not their specific dynamics. As the allocation generates actuator velocity commands, adopting first order actuator dynamics naturally follows our formulation. Assuming second order actuator dynamics would require an additional differentiation step of Eq. (13), as well as propeller acceleration feedback, which is not commonly available with current Electronic Speed Controllers (ESCs). For this reason, we assume first order dynamics

$$\dot{\mathbf{q}} = -\mathbf{K}\mathbf{q}_e, \quad (15)$$

where $\mathbf{K} \in \mathbb{R}^{2N \times 2N}$ is a positive-definite and diagonal gain matrix, and $\mathbf{q}_e \in \mathbb{R}^{2N}$ is a vector of joint position errors (angular position errors for the tilt arms and rotation speed errors for the propellers). To include the dynamics into the allocation problem, one can solve the normalized allocation in Eq. (13), de-normalize the actuators' velocity commands with Eq. (9) and then invert the dynamics in Eq. (15) to obtain the desired tilt angles position command and propellers velocity command based on the current actuator feedback.

Another important advantage of the normalized allocation is that it's independent of the actuators' dynamics: the minimum norm solution obtained from Eq. (13) only depends on the maximum actuator velocity, and not on Eq. (15). Thus, changes in the actuator dynamics do not affect the allocation itself, but only the last dynamics inversion step. All the steps of the proposed allocation process are summarized in Fig. 4.

VII. AUGMENTED DIFFERENTIAL ALLOCATION WITH LIMIT CURVES (DLC)

While the dynamics aware allocation in Section VI improves upon the augmented allocation in Section V by taking into account the actuators dynamics and their control limits, it still does not address the problem of joint position limits (minimum and maximum arm angles and rotor speeds). This might not be a problem for the tilt arms, which could virtually rotate indefinitely depending on their mechanical implementation. However, it definitely affects the propellers' speeds as their limit depends on the maximum power that the ESCs can provide, propeller's length and pitch. Notice that, while in Section VI we were referring to the acceleration limits on the propellers, we now address the problem of speed limits,

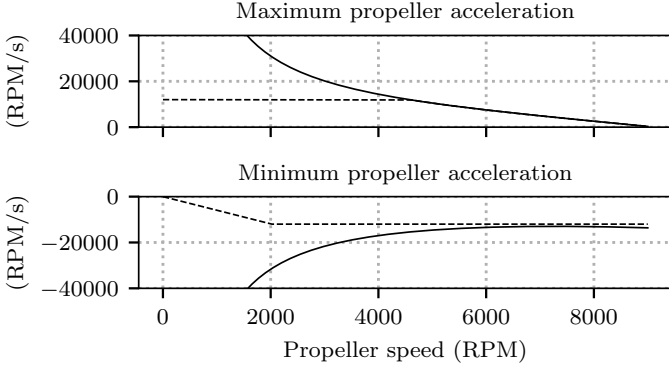


Fig. 5: Example acceleration limit curves (solid lines) from the propellers power balance in Eq. (16). The dashed lines represent the saturated versions of the curves, where the maximum and minimum accelerations have been capped to represent the internal software ESC limits. For very low propeller speeds, the drag torque has a very low effect, leading to very high acceleration and deceleration limits. As speed increases, the quadratic drag force overtakes the electrical torque, leading to a reduction in the maximum acceleration and deceleration, until the acceleration becomes zero when the propeller reaches the maximum speed. The curves were obtained with $\eta = 0.8$, $V = 23V$, $\bar{I} = -\underline{I} = 17A$, $J = 4.5e^{-4}Kg m^2$, $d = 3.5e^{-7}Nms^2$ and $\bar{\omega} = -\underline{\omega} = 1.3e^4RPM/s$.

which directly relates to the maximum thrust that a propeller can generate.

To guarantee these speed limits, we propose to embed the propeller limit curves into the allocation description. The limit curves represent the maximum and minimum acceleration a propeller can generate, depending on its speed. For example, as a propeller approaches its maximum speed, its maximum acceleration will reduce until zero. On the other hand, when slowing down, the maximum acceleration will reach its peak.

In the following, we provide a model that shows the state-dependency of such limit curves and how they are used to balance propeller speeds without the need for an additional secondary allocation goal.

A. Real Propeller Limit Curves

The propeller limit curves for a generic propeller motor can be obtained through the power equilibrium equation. Specifically, the input electrical power must be equal to the power dissipated to fight the propeller's inertia and drag torque. This translates to

$$\eta VI = J\omega\dot{\omega} + d\omega^3, \quad (16)$$

where all the quantities are scalar and $\eta < 1$ is the electrical efficiency of the motor, V is the voltage provided to the ESC, I is the current absorbed by the motor, J is the propeller and rotor combined inertia and d is the drag coefficient. If we consider \bar{I} the maximum current the ESC is able to provide, we can rewrite Eq. (16) to obtain the maximum propeller acceleration

$$\bar{\omega} = \frac{\eta V \bar{I}}{J} \frac{1}{\omega} - \frac{d}{J} \omega^2. \quad (17)$$

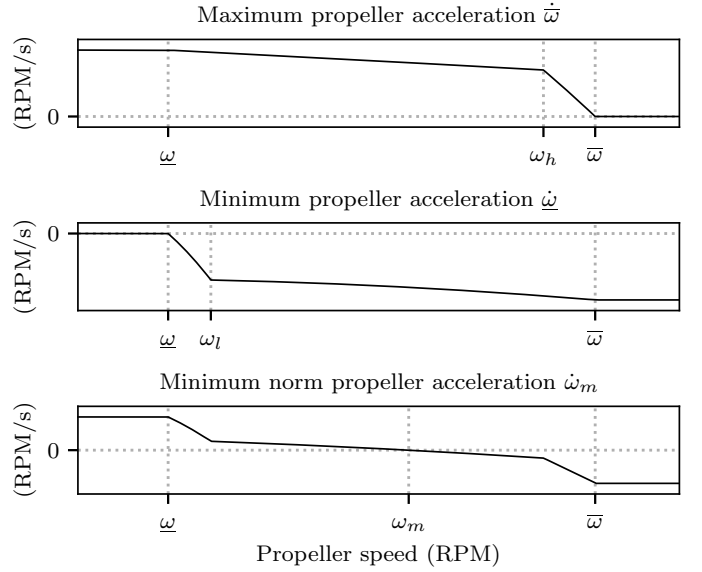


Fig. 6: Proposed propeller limit curves. This approximation allows arbitrarily choosing the equilibrium speed ω_m of the propellers.

Similarly, the minimum acceleration $\underline{\omega}$ can be obtained by substituting the minimum current \underline{I} in Eq. (17).

An example of these curves for our propeller-ESC combination is shown in Fig. 5 (solid line). While these curves fit well the real propeller behavior at high speeds where the actual physical power expenditure is dominating, at lower speeds the ESC control algorithm and other losses are more apparent:

- Most multirotors are not designed to have their propellers spin backward, which means that the minimum acceleration $\underline{\omega}$ should actually go to zero as the speed approaches the minimum $\underline{\omega}$ (usually zero).
- The maximum acceleration is not only limited by the maximum current and drag torque but also by the ESC internal controller. This means that the maximum acceleration should also saturate to $\bar{\omega}$ as the speed approaches the minimum $\underline{\omega}$.

We illustrate these modified acceleration limits in Fig. 5 as dashed lines.

B. Propellers' Equilibrium Speed and Proposed Limit Curves

With the proposed limit curves model, we aim to mimic the shape of the real curves, but most importantly give the design freedom to arbitrarily choose the value of the propellers equilibrium speed, which we define as the velocity ω_m whose mean acceleration limit is zero, as

$$\dot{\omega}_m(\omega_m) = \frac{\bar{\omega}(\omega_m) + \underline{\omega}(\omega_m)}{2} = 0. \quad (18)$$

Equally distributing the thrust among propellers is particularly important for tiltrotor aerial vehicles as, at high pitch/roll angles, some propellers might spin much faster than others. When back to horizontal hover, if nothing brings the propeller speeds down, the resulting propellers configuration can be highly power inefficient, unnecessarily bringing the actuators

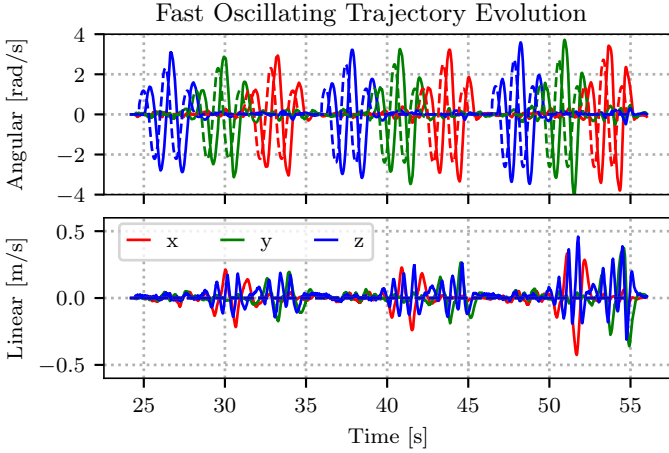


Fig. 7: Time trajectory of three increasingly fast oscillations (1.3s to 1.1s). The dashed line is the reference speed while the solid line is the actual speed along the body axes. The reference linear speed is zero, but linear motions still happen because of the very fast angular oscillations. Here is shown the performance of DLC for reference.

close to saturation. With the equilibrium speed as a tunable parameters, we can set it very low for energy efficiency, or higher than hovering speed if more internal forces and a faster dynamic response are desired. The minimum norm solution of the allocation problem in Eq. (13) will passively drive the propeller speed to the desired equilibrium point ω_m , removing the need for secondary nullspace allocation goals to balance propeller speeds.

Keeping these requirements in mind, we propose to model the maximum and minimum acceleration curves as composed of two pieces each, as shown in Fig. 6

$$\bar{\omega}(\omega) = \begin{cases} c_{0,0}\omega + c_{0,1}\omega^2 + c_{0,2}, & \forall \omega \in [\underline{\omega}, \omega_h] \\ c_{1,0}\omega^2 + c_{1,1}, & \forall \omega \in [\omega_h, \bar{\omega}] \end{cases} \quad (19)$$

$$\underline{\omega}(\omega) = \begin{cases} c_{2,0}\omega^2 + c_{2,1}, & \forall \omega \in [\underline{\omega}, \omega_l] \\ c_{3,0}\omega^2 + c_{3,1}, & \forall \omega \in [\omega_l, \bar{\omega}] \end{cases} \quad (20)$$

where ω_h and ω_l are two arbitrary propeller speeds in which we start ramping down the maximum acceleration and ramping up the minimum acceleration, respectively.

With their 7 coefficients, the curves are uniquely identified once the maximum/minimum speeds and accelerations are chosen, together with the equilibrium speed. To have the rotor speeds converge to ω_m , we design our curves such that the minimum norm acceleration solution $\dot{\omega}_m$ is positive if $\omega < \omega_m$, pushing the propeller to accelerate towards ω_m , or negative if $\omega > \omega_m$. Recomputing the new limits requires the solution of a small linear system of equations which is detailed in Appendix A. Then, the new limits can be applied by just recomputing the scaling matrix and bias vector in Eq. (10).

VIII. EXPERIMENTAL COMPARISON

To compare the five different allocation methods of Fig. 3, we fly the robot through seven different trajectories: a slow Figure-8 and six increasingly fast and dynamic trajectories that

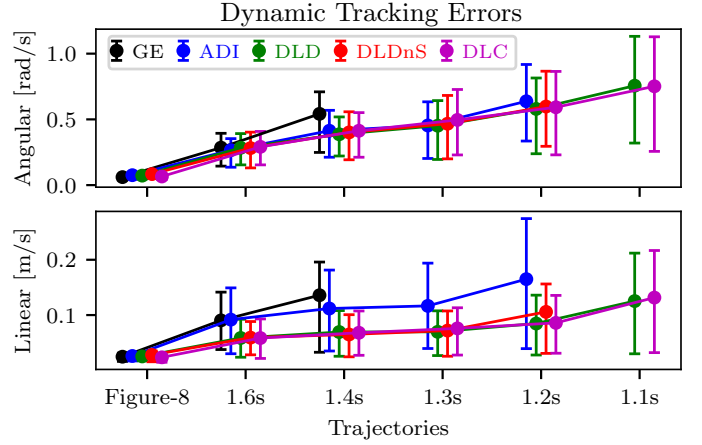


Fig. 8: Mean and quartiles of the linear and angular tracking velocity errors achieved by the six allocation methods. When data from an allocation is missing for a specific trajectory, it means that the method failed to complete the trajectory. The use of actuator dynamics allows the two methods DLC and DLD to complete all trajectories.

involve different rotations on the spot. While the Figure-8 was already used as a benchmark in other works [2], [8], the other five increasing fast trajectory require the platform to follow fast sinusoidal roll, pitch and yaw motions up to 4 rad s^{-1} , as shown in Fig. 7.

We are mostly interested in answering three questions:

- Which allocation methods are dynamic enough to handle fast rotation/translation, and how much improvement does moving from geometric to differential allocation and including the actuator dynamics bring?
- How do geometric and differential methods compare in terms of energy efficiency?
- Do some methods stress the actuators more than others?

For each trajectory we evaluate the pose and velocity tracking errors, as well as the actuators' usage and power consumption, which we present in the following sections.

A. Trajectory tracking

In Table I we summarize the success of each allocation method in completing the desired trajectories, eventually bringing all of them to failure. A method is successful independently of its linear/angular tracking errors, as long as the controller does not diverge. The first to fail is the GE, which completes the Figure-8 and only the first of the oscillating trajectories. This was expected as this method assumes instantaneous control of the actuators, without any knowledge of actuator dynamics and limits. The second method to fail is the ADI, which completes most of the proposed trajectories. Despite not having knowledge of the exact actuator dynamics and limits, this method still performs comparably well, although it is highly dependent on a careful tuning of the weight matrix \mathbf{W} to balance the actuator's usage. Once we introduce the actuator dynamics and limits, getting rid of the weight matrix \mathbf{W} , the DLD obtains the best performance, only failing on the very last trajectory. However, notice that both ADI and DLD rely on the

	Fig-8	1.6 s	1.4 s	1.3 s	1.2 s	1.1 s	1.0 s
GE							
ADI							
DLD							
DLdNS							
DLC							
Ang. vel.	0.5	2.3	2.8	3.2	3.5	4.0	-
Lin. vel.	0.4	0.17	0.20	0.25	0.35	0.6	-

TABLE I: The table summarizes whether an allocation method was successful in completing the desired trajectory (green) or not (red). Allocation methods are on the rows while the trajectories are on the columns slowest (left) to fastest (right). The best methods (DLC and DLD) require the use of actuator dynamics. The last two rows show the maximum linear (m s^{-1}) and angular (rad s^{-1}) body velocity norms reached during the corresponding trajectory.

secondary objective in Eq. (6) to balance the propeller speeds and avoid actuator saturation during flight. This can be quite inefficient as the nullspace of the allocation problem is always full, putting additional burden on the actuators even just for free flying. The moment we remove this nullspace objective in the Augmented Differential allocation with Dynamics but No Secondary Objectives (DLdNS), we notice a decrease in performance, as the propellers' speed starts getting closer to its limit during the flight. By integrating the propeller limits derived from their power balance in Section VII-B, the DLC recovers the performance boost introduced with the actuator dynamics in DLD, but keeping the nullspace completely free for other possible tasks.

These results are confirmed in Fig. 8, where the mean and quartiles of the linear and angular tracking velocity errors are shown. Here we focus specifically on dynamic tracking errors as we are interested in the dynamic performance of these allocation methods, but a full statistical overview of the tracking errors (including position and attitude) is available in Fig. 14 later in the Appendix. While the angular performance is mostly similar between the different methods (unless they fail the trajectory), the linear errors show a clear separation between the methods that use actuator dynamics and those that do not. Our intuition is that the linear dynamics are primarily influenced by the arm servomotors rather than the propellers. Since servomotors typically exhibit slower dynamics, neglecting them explicitly tends to have the greatest impact on linear errors.

Again, the two methods that provide the best results are DLD and DLC, despite having a main difference in keeping the propellers' speeds balanced: one uses secondary objectives and the other only limit curves. In particular, we use the Welch's unequal variances T-test to evaluate whether there is any statistically significant difference between the two. We assume as a null hypothesis that the two error distributions have identical average values, and we reject the null hypothesis if the p-value is less than 0.05. The results show that the two methods are statistically very similar with p-values of 0.106 for the linear and even 0.788 for the angular tracking errors. This implies that by using the propellers' acceleration limits derived

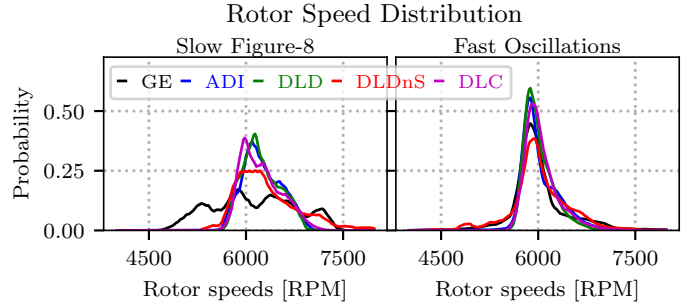


Fig. 9: Comparison of rotor speeds distributions between the different allocation methods. When the secondary objective is not present (DLdNS) or in case of the geometric allocation (GE), the rotor speeds distribution is wider and the propellers are pushed closer to their limits.

from their power balance, the actuator dynamics can be fully utilized without requiring additional secondary objectives, and without compromising performance.

After evaluating the tracking performance, in the next section we focus on how the different allocation methods utilize their actuators, which affects their power consumption.

B. Actuators' usage and power consumption

In Fig. 9 we compare the rotor speeds distributions between the different allocation methods. We would ideally keep the propeller speed around 5800 RPM , as that is the hovering speed for our system. Most allocation methods manage to keep the propeller speeds balanced around the desired value thanks to either a secondary command or the use of limit curves. However, when the secondary objective is not present or in case of GE or DLdNS, the rotor speeds distribution is wider and the propellers are pushed closer to their limits. Indeed, GE will always find the most energy efficient configuration by design, which might be a different propeller speed depending on the robot's orientation. On the other hand, DLdNS does not care about the actual propeller speeds, but only their acceleration such to generate the desired jerk command.

In Fig. 10 we investigate how much the different rotor speed distributions affect the power efficiency of the allocations (as power increases cubically with the propeller speed). We are curious whether methods that achieve higher trajectory track-

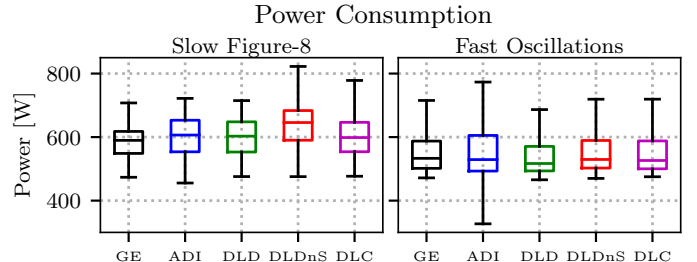


Fig. 10: Propellers power consumption between the different allocation methods. The average consumption differs up to 2% between the different allocation methods, apart from DLdNS which uses 8% more power on average on slow trajectory.

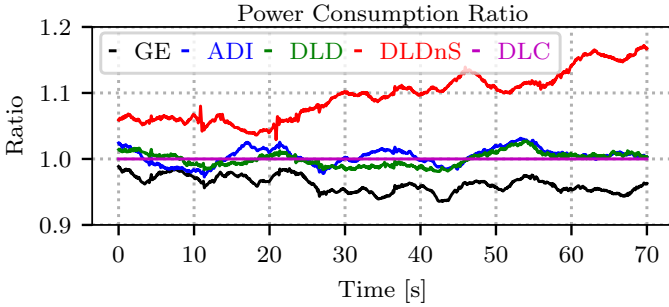


Fig. 11: Power usage ratio between DLC and the other allocation methods during the slow Figure-8 trajectory. GE is up to 6% more efficient than the other differential methods, which have similar consumptions. DLDnS increases the average propeller speeds over time, leading to a power consumption up to 18% higher than the DLC method.

ing performance also result in increased power consumption. In practice, we observe little difference between the various methods (power consumption differs up to $\pm 2\%$), although DLDnS uses 8% more power on average on the slow trajectory. This is due to the propellers saturating over time, as the allocation has no secondary task to keep the speeds low, leading to a higher power consumption. To better demonstrate this, we show in Fig. 11 the power usage ratio between our proposed DLC and the other methods during the slow Figure-8 trajectory. As time progresses, the DLDnS method increases the average propeller speeds, leading to a power consumption up to 18% higher than the DLC method. This means that, when using a differential allocation method, either a secondary task or propeller limit curves are necessary to properly balance the actuators' usage. At the same time we observe how GE is up to 6% more efficient, as it always tries to align the propellers against the gravity vector by design, minimizing the amount of energy wasted in internal forces. Unfortunately, since this method allocates its actuators instantaneously without taking into account any dynamics, this gain in power efficiency comes at the cost of dynamics tracking performance, as we show in Section VIII-A.

IX. STOPPING PROPELLERS

Here we demonstrate with a qualitative demo how to use DLC with the propeller's limit curves to stop one or more propellers in-flight. At the same time we use the free nullspace of the allocation to control the rotation of the arms. In Fig. 12 we show how the propellers are commanded to slow down until they stop, and then the tilt motors are commanded to follow a 0.5 rad s^{-1} velocity reference. This is possible as we take the limit curves in Fig. 6 and make the propeller maximum acceleration limit negative, forcing the allocation to decelerate the propeller, until it stops. After a few seconds, the limits are released and the allocation naturally brings back the propellers to hovering speed to balance the propellers' usage. Also, we observe a clear difference in tilt motor commands when they are used freely for flight versus when we actively set them to 0 or 0.5 rad s^{-1} . The stopping and reactivation of the propellers is also in Fig. 13.

In addition to the trajectory tracking performance shown in Section VIII, DLC leaves the full null space of the system free to control the arms. This, coupled to the possibility of turning off the propellers at will, opens the door to: (i) a safer interaction with the environment, since the propellers close to a surface can be just disabled; (ii) additional manipulation capabilities, as the rotating arms of the disabled propellers could be used for active interaction, such as screwing a bolt into a wall.

X. CONCLUSION

In this work, we demonstrate several actuator allocation methods, comparing them not only from a dynamic tracking perspective but also in terms of actuator and power usage. We show the limitations of geometric allocation, how differential allocation can overcome them, and how to further improve it by taking into account the actuator dynamics and limits. We introduce the concept of propeller limit curves, which define

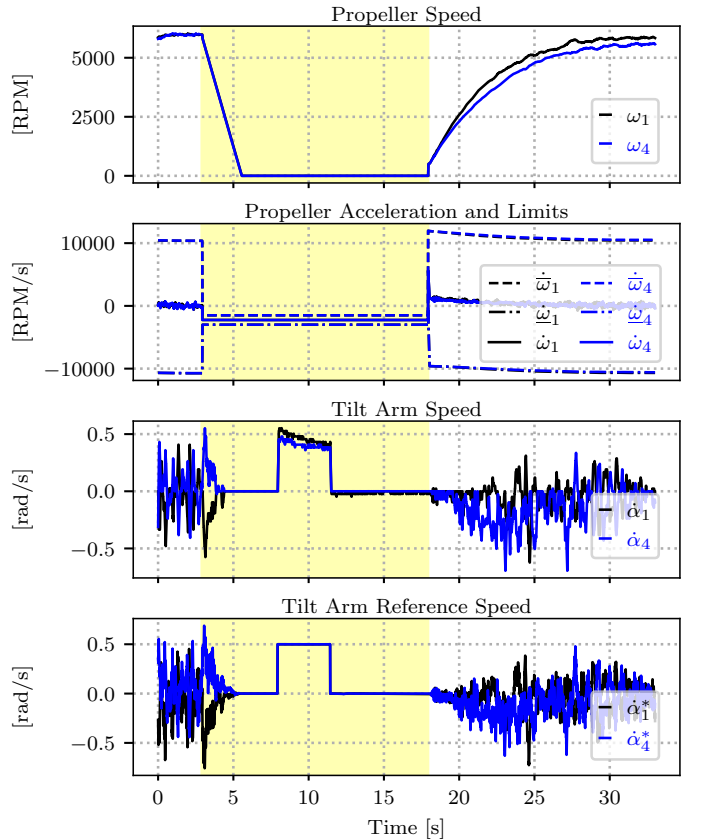


Fig. 12: Top to bottom: the speeds of the two propellers, the commanded propeller accelerations (and their limits as dashed lines), the tilt speeds of the two servomotors, and the commanded tilt speeds. When the acceleration limits are both negative, the propellers slow down until they stop. After a few seconds the tilt motors are commanded to follow a 0.5 rad s^{-1} velocity reference. Then the limits are released and the allocation naturally brings back the propellers to hovering speed to balance the propellers' usage. The yellow shaded area highlights when the motors are commanded to turn off and we generate a specific velocity command for the tilt angles.



Fig. 13: From left to right: the Aerial Robot is hovering in place, then the propellers are commanded to stop and the arms to rotate. Finally the propellers are enabled again and the arms slowly align with gravity again to balance the actuators' usage. The stopped propellers are highlighted in yellow.

their acceleration limits as a function of their speed and can be used to balance the propellers' speeds without the need for secondary allocation goals. At the same time, they can be used to stop propellers in-flight, allowing the platform to control its propelling arms as manipulation tools, possibly removing the need for additional manipulation arms. For example, the arm rotation could be used to screw a bolt in a wall, or a light bulb into a socket. The propeller stopping could also make the platform more crash resilient: if a propeller gets damaged, the corresponding motor can be stopped without affecting the overall flight performance. Importantly, these improvements are still compatible with existing wrench control architectures, without the need for acceleration feedback. Moreover the different allocation methods are built upon each other. We show that dynamic performance can improve with the use of actuator dynamics and power curves, tracking more dynamic oscillating trajectories with angular velocities up to 4 rad s^{-1} . At the same time, removing the necessity of acceleration feedback present in the state-of-the-art, we demonstrate that a basic differential allocation can still be sufficient for most motions, in case the actuator models are not available.

APPENDIX

COMPUTING THE PROPELLER LIMIT CURVES

The 7 coefficients of the power curves can be computed by solving the following linear system of equations

$$\bar{\omega}(\underline{\omega}) = c_{0,0}\underline{\omega} + c_{0,1}\underline{\omega}^2 + c_{0,2}, \quad (21a)$$

$$c_{0,0}\omega_h + c_{0,1}\omega_h^2 + c_{0,2} = c_{1,0}\omega_h^2 + c_{1,1}, \quad (21b)$$

$$0 = c_{1,0}\bar{\omega}^2 + c_{1,1}, \quad (21c)$$

$$\dot{\omega}_1 = c_{1,0}\omega_h^2 + c_{1,1}, \quad (21d)$$

$$0 = c_{2,0}\underline{\omega}^2 + c_{2,1}, \quad (21e)$$

$$c_{2,0}\omega_l^2 + c_{2,1} = c_{3,0}\omega_l^2 + c_{3,1}, \quad (21f)$$

$$\omega_2 = c_{2,0}\omega_l^2 + c_{2,1}, \quad (21g)$$

$$\underline{\dot{\omega}}(\bar{\omega}) = c_{3,0}\bar{\omega}^2 + c_{3,1}, \quad (21h)$$

$$0 = c_{0,0}\omega_m + c_{0,1}\omega_m^2 + c_{0,2} + c_{3,0}\omega_m\omega_m^2 + c_{3,1}. \quad (21i)$$

This system has a unique solution for the coefficients $c_{i,j}$, given the values of the minimum and maximum propeller speeds $\underline{\omega}$, $\bar{\omega}$, and accelerations $\bar{\omega}(\underline{\omega})$, $\underline{\dot{\omega}}(\bar{\omega})$, the speed at which the quadratic drag effect becomes predominant ω_h and its acceleration $\bar{\omega}(\omega_h)$, the speed at which we start saturating the propeller acceleration to avoid reducing its speed below 0 ω_l and its acceleration $\underline{\dot{\omega}}(\omega_l)$, and last the desired average propeller speed ω_m .

In our experiments, we set the desired average propeller speed ω_m to be the hovering speed 5800 RPM , while the minimum speed $\underline{\omega}$ is 0 and the maximum $\bar{\omega}$ is 8700 RPM . In our experience, the acceleration of the propeller starts noticeably decreasing when approaching $\sim 8000 \text{ RPM}$. For this reason, we decided to use $\omega_l = 7800 \text{ RPM}$, which corresponds to 90% of the total speed range. The lower limit ω_h does not come from the power equilibrium but it's rather a limitation of the ESC since the speed cannot go below 0. For symmetry we choose it to be 900 RPM , corresponding to 10% of the total speed range. The maximum and minimum accelerations in those points $\bar{\omega}(\omega_h)$ and $\underline{\dot{\omega}}(\omega_l)$ are set to the 80% of the absolute maximum and minimum acceleration limits of the propellers $\bar{\omega}(\underline{\omega})$, $\underline{\dot{\omega}}(\bar{\omega})$. These highly depend on the ESC's limitations and need to be found experimentally. In our case, we have $\bar{\omega}(\underline{\omega}) = 12000 \text{ RPM/s}$ and $\underline{\dot{\omega}}(\bar{\omega}) = -14000 \text{ RPM/s}$.

We can then compute the curves coefficients vector $\mathbf{c} = [c_{0,0}, c_{0,1}, c_{0,2}, c_{1,0}, c_{1,1}, c_{2,0}, c_{2,1}, c_{3,0}, c_{3,1}]$ with

$$\mathbf{c} = \mathbf{A}^{-1}\mathbf{b}, \quad (22)$$

where $\mathbf{b} = [\bar{\omega}(\underline{\omega}), 0, 0, \dot{\omega}_1, 0, 0, \dot{\omega}_2, \underline{\dot{\omega}}(\bar{\omega}), 0]$ and

$$\mathbf{A} = \begin{bmatrix} \underline{\omega} & \underline{\omega}^2 & 1 & 0 & 0 & 0 & 0 & 0 & 0 \\ \omega_h & \omega_h^2 & 1 & -\omega_h^2 & -1 & 0 & 0 & 0 & 0 \\ 0 & 0 & 0 & \bar{\omega}^2 & 1 & 0 & 0 & 0 & 0 \\ 0 & 0 & 0 & \dot{\omega}_1^2 & 1 & 0 & 0 & 0 & 0 \\ 0 & 0 & 0 & 0 & 0 & \omega_l^2 & 1 & 0 & 0 \\ 0 & 0 & 0 & 0 & 0 & \omega_l^2 & 1 & -\omega_l^2 & -1 \\ 0 & 0 & 0 & 0 & 0 & \omega_l^2 & 1 & 0 & 0 \\ 0 & 0 & 0 & 0 & 0 & 0 & 0 & \bar{\omega}^2 & 1 \\ \omega_m & \omega_m^2 & 1 & 0 & 0 & 0 & 0 & \omega_m^2 & 1 \end{bmatrix}.$$

Notice how Eq. (22) is a relatively small matrix inversion which can be computed in real-time. Also the values of minimum and maximum acceleration can be changed arbitrarily, for example both can be put negative to stop the propellers in-flight, or restored to their original values once the propellers can be turned on again.

REFERENCES

- [1] A. Ollero, M. Tognon, A. Suarez, D. Lee, and A. Franchi, "Past, present, and future of aerial robotic manipulators," *IEEE Transactions on Robotics*, vol. 38, no. 1, pp. 626–645, 2022.
- [2] K. Bodie, M. Brunner, M. Pantic, S. Walsler, P. Pfändler, U. Angst, R. Siegwart, and J. Nieto, "Active interaction force control for contact-based inspection with a fully actuated aerial vehicle," *IEEE Transactions on Robotics*, vol. 37, no. 3, pp. 709–722, 2021.

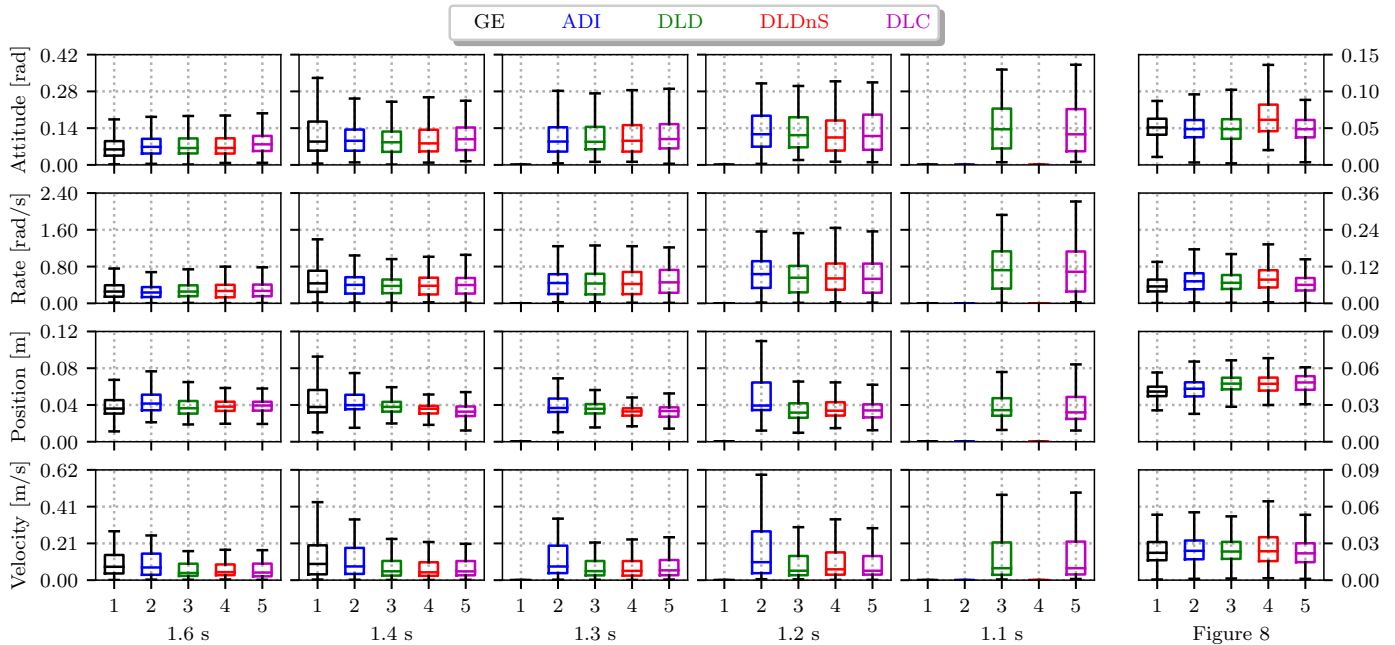


Fig. 14: Boxplots comparison of the tracking results from the different allocation methods on several test trajectories. From top to bottom row: Attitude, Angular Velocity, Position and Linear Velocity errors. The five columns on the left show the results with increasingly fast sinusoidal trajectories, from a period of 1.6 s to 1.1 s. The additional column on the right shows the results with a slow Figure-8 trajectory. If no data is present, the corresponding allocation method diverged while following the trajectory.

- [3] S. Park, J. Lee, J. Ahn, M. Kim, J. Her, G.-H. Yang, and D. Lee, "Odor: Aerial manipulation platform enabling omnidirectional wrench generation," *IEEE/ASME Transactions on Mechatronics*, vol. 23, no. 4, pp. 1907–1918, 2018.
- [4] M. Tognon, H. A. T. Chávez, E. Gasparin, Q. Sablé, D. Bicego, A. Mallet, M. Lany, G. Santi, B. Revaz, J. Cortés, and A. Franchi, "A truly-redundant aerial manipulator system with application to push-and-slide inspection in industrial plants," *IEEE Robotics and Automation Letters*, vol. 4, no. 2, pp. 1846–1851, 2019.
- [5] M. Ryll, G. Muscio, F. Pierri, E. Cataldi, G. Antonelli, F. Caccavale, D. Bicego, and A. Franchi, "6d interaction control with aerial robots: The flying end-effector paradigm," *The International Journal of Robotics Research*, vol. 38, no. 9, pp. 1045–1062, 2019. [Online]. Available: <https://doi.org/10.1177/0278364919856694>
- [6] D. Brescianini and R. D'Andrea, "Design, modeling and control of an omni-directional aerial vehicle," in *2016 IEEE International Conference on Robotics and Automation (ICRA)*, 2016.
- [7] E. Cuniato, C. Geckeler, M. Brunner, D. Strübin, E. Bähler, F. Ospelt, M. Tognon, S. Mintchev, and R. Siegwart, "Design and control of a micro overactuated aerial robot with an origami delta manipulator," in *2023 IEEE International Conference on Robotics and Automation (ICRA)*, 2023, pp. 5352–5358.
- [8] M. Allenspach, K. Bodie, M. Brunner, L. Rinsoz, Z. Taylor, M. Kamel, R. Siegwart, and J. Nieto, "Design and optimal control of a tiltrotor micro-aerial vehicle for efficient omnidirectional flight," *The International Journal of Robotics Research*, vol. 39, no. 10-11, pp. 1305–1325, 2020.
- [9] M. Ryll, D. Bicego, M. Giurato, M. Lovera, and A. Franchi, "Fast-hex - A morphing hexarotor: Design, mechanical implementation, control and experimental validation," *CoRR*, vol. abs/2004.06612, 2020. [Online]. Available: <https://arxiv.org/abs/2004.06612>
- [10] J. T. M. W. Mueller, J. Tang, and M. W. Mueller, "Pairtilt: Design and control of an active tilt-rotor quad-copter for improved efficiency and agility."
- [11] M. Brunner, G. Rizzi, M. Studiger, R. Siegwart, and M. Tognon, "A planning-and-control framework for aerial manipulation of articulated objects," *IEEE Robotics and Automation Letters*, vol. 7, no. 4, pp. 10 689–10 696, 2022.
- [12] R. Falconi and C. Melchiorri, "Dynamic model and control of an over-actuated quadrotor uav," *IFAC Proceedings Volumes*, vol. 45, no. 22, pp. 192–197, 2012, 10th IFAC Symposium on Robot Control. [Online]. Available: <https://www.sciencedirect.com/science/article/pii/S1474667016336096>
- [13] M. Ryll, H. H. Bühlhoff, and P. R. Giordano, "A novel overactuated quadrotor unmanned aerial vehicle: Modeling, control, and experimental validation," *IEEE Transactions on Control Systems Technology*, vol. 23, no. 2, pp. 540–556, 2015.
- [14] Z. Qin, J. Wei, M. Cao, B. Chen, K. Li, and K. Liu, "Design and flight control of a novel tilt-rotor octocopter using passive hinges," *IEEE Robotics and Automation Letters*, 2023.
- [15] S. Rajappa, M. Ryll, H. H. Bühlhoff, and A. Franchi, "Modeling, control and design optimization for a fully-actuated hexarotor aerial vehicle with tilted propellers," in *2015 IEEE International Conference on Robotics and Automation (ICRA)*, 2015, pp. 4006–4013.
- [16] M. Ryll, D. Bicego, and A. Franchi, "Modeling and control of fast-hex: A fully-actuated by synchronized-tilting hexarotor," in *2016 IEEE/RSJ International Conference on Intelligent Robots and Systems (IROS)*, 2016, pp. 1689–1694.
- [17] —, "A truly redundant aerial manipulator exploiting a multi-directional thrust base," *IFAC-PapersOnLine*, vol. 51, no. 22, pp. 138–143, 2018, 12th IFAC Symposium on Robot Control SYROCO 2018. [Online]. Available: <https://www.sciencedirect.com/science/article/pii/S2405896318332373>
- [18] F. Morbidi, D. Bicego, M. Ryll, and A. Franchi, "Energy-efficient trajectory generation for a hexarotor with dual-tilting propellers," in *2018 IEEE/RSJ International Conference on Intelligent Robots and Systems (IROS)*, 2018, pp. 6226–6232.
- [19] K. Bodie, Z. Taylor, M. Kamel, and R. Siegwart, "Towards efficient full pose omnidirectionality with overactuated MAVs," in *Springer Proceedings in Advanced Robotics*. Springer International Publishing, 2020, pp. 85–95. [Online]. Available: <https://doi.org/10.48550/arXiv.1810.06258>
- [20] T. A. Johansen and T. I. Fossen, "Control allocation—a survey," *Automatica*, vol. 49, no. 5, pp. 1087–1103, 2013. [Online]. Available: <https://www.sciencedirect.com/science/article/pii/S0005109813000368>
- [21] J. Sugihara, M. Zhao, T. Nishio, K. Okada, and M. Inaba, "Beetle—self-reconfigurable aerial robot: Design, control and experimental validation," *IEEE/ASME Transactions on Mechatronics*, 2024.
- [22] M. Zhao, K. Okada, and M. Inaba, "Versatile articulated aerial robot dragon: Aerial manipulation and grasping by vectorable thrust control,"

The International Journal of Robotics Research, vol. 42, no. 4-5, pp. 214–248, 2023.

- [23] T. Nishio, M. Zhao, K. Okada, and M. Inaba, “Design, control, and motion-planning for a root-perching rotor-distributed manipulator,” *IEEE Transactions on Robotics*, 2023.
- [24] G. Notomista, S. Mayya, M. Selvaggio, M. Santos, and C. Secchi, “A set-theoretic approach to multi-task execution and prioritization,” in *2020 IEEE International Conference on Robotics and Automation (ICRA)*. IEEE, 2020, pp. 9873–9879.
- [25] C. Lanegger, M. Pantic, R. Bähnmann, R. Siegwart, and L. Ott, “Chasing millimeters: design, navigation and state estimation for precise in-flight marking on ceilings,” *Autonomous Robots*, vol. 47, no. 8, pp. 1405–1418, 2023.
- [26] K. Bodie, Z. Taylor, M. Kamel, and R. Siegwart, “Towards efficient full pose omnidirectionality with overactuated mavs,” in *Proceedings of the 2018 International Symposium on Experimental Robotics*. Springer, 2020, pp. 85–95.
- [27] B. Siciliano, O. Khatib, and T. Kröger, *Springer handbook of robotics*. Springer, 2008, vol. 200.
- [28] A. D. Ames, G. Notomista, Y. Wardi, and M. Egerstedt, “Integral control barrier functions for dynamically defined control laws,” *IEEE Control Systems Letters*, vol. 5, no. 3, pp. 887–892, 2020.
- [29] E. Cuniato, N. Lawrance, M. Tognon, and R. Siegwart, “Power-based safety layer for aerial vehicles in physical interaction using lyapunov exponents,” *IEEE Robotics and Automation Letters*, vol. 7, no. 3, pp. 6774–6781, 2022.
- [30] K. Bodie, M. Brunner, M. Pantic, S. Walser, P. Pfändler, U. Angst, R. Siegwart, and J. Nieto, “Active interaction force control for contact-based inspection with a fully actuated aerial vehicle,” *IEEE Transactions on Robotics*, vol. 37, no. 3, pp. 709–722, 2020.



Helen Oleynikova is also a Senior Researcher in the Autonomous Systems Lab (ASL) at ETH Zurich focusing on volumetric mapping and planning for both manipulation and flying robots.



Roland Siegwart is professor for autonomous mobile robots at ETH Zurich, founding co-director of the technology transfer center Wyss Zurich and board member of multiple high tech companies. He studied mechanical engineering at ETH Zurich, spent ten years as professor at EPFL Lausanne (1996 – 2006), held visiting positions at Stanford University and NASA Ames and was Vice President of ETH Zurich (2010-2014). He is IEEE Fellow and recipient of the IEEE RAS Pioneer Award and IEEE RAS Inaba Technical Award. He is among the most cited scientist in robots world-wide, co-founder of more than half a dozen spin-off companies and a strong promoter of innovation and entrepreneurship in Switzerland. His interests are in the design, control and navigation of flying, wheeled and walking robots operating in complex and highly dynamical environments.



Eugenio Cuniato (Graduate Student Member, IEEE) is currently pursuing a Ph.D. degree at the Autonomous Systems Lab, ETH Zurich, Switzerland with a Marie Skłodowska-Curie (MSCA) scholarship. His research focus is on control of aerial manipulators for high-performance aerial physical interaction.



Michael Pantic is a Senior Researcher at the Autonomous Systems Lab (ASL) at ETH Zurich focusing on system architecture, perception and navigation for aerial robots.



Mike Allenspach received his Master degree in Robotics, Systems and Control in 2020 from ETH Zurich, Switzerland. He is currently pursuing a Ph.D. degree at the Autonomous Systems Lab at ETH Zurich. His research interests include planning and control for aerial manipulation, especially the integration of human-robot interaction.



Thomas Stastny is currently a Senior Researcher in the Autonomous Systems Lab (ASL) at ETH Zurich focusing on learning-based perception and control for omnidirectional aerial manipulators.